Rare Met. (2022) 41(4):1314–1322
https://doi.org/10.1007/s12598-021-01877-z

RARE METALS

ORIGINAL ARTICLE

Morphology-controlled growth of large-area $PtSe_2$ films for enhanced hydrogen evolution reaction

Rui Hao, Qing-Liang Feng*, Xiao-Jian Wang, Yi-Chen Zhang, Kan-She Li*

Received: 13 August 2021 / Revised: 8 September 2021 / Accepted: 9 September 2021 / Published online: 24 December 2021

Abstract Transition metal dichalcogenides (TMDs) have emerged as a promising electrocatalyst for hydrogen evolution reaction (HER) due to its excellent conductivity and abundant electrocatalytic active sites of its edges. TMDs nanowall can expose abundant of edges so that they tend to show better catalytic performance for hydrogen evolution reaction. Herein, $PtSe_2$ nanowall films with morphology controlled at centimeters level are synthesized by selenizing Pt film. The dynamic and thermodynamics of selenation reaction are investigated. The nanowall structure can be obtained by controlling the growth temperature, and the thickness of nanowall can be tuned by the original thickness of Pt film. The Pt atoms can be rearranged into ordered distribution at 550 °C and can be induced to well-ordered $PtSe_2$ nanowalls finally. The well-ordered $PtSe_2$ nanowall films show excellent HER performance, with an overpotential of 0.3 V at -10 mA·cm^{-2} and a Tafel slope of $\sim$52 mV·dec^{-1}. This work demonstrates the great potential of activated 2D $PtSe_2$ as an ultrathin film catalyst for the HER, which is valuable to provide instruction and afford experience for further application at industrial level.

Keywords Large area; $PtSe_2$; Nanowall; Morphology controlled; HER

1 Introduction

Owing to the special and outstanding material properties (e.g., tunable band gap [1], high carrier mobility [2], excellent mechanic [3], and tunable carrier density and polarity [4]), two-dimensional (2D) materials have received significant interest in recent decades. Preparation of large-scale and high-quality two-dimensional crystals is foundation for its further application in next-generation electronic devices [5, 6], while transition metal dichalcogenide (TMD) materials are also shown for excellent catalytic activity for many important electrochemical reactions due to unsaturated bond at the edge of crystals, such as hydrogen evolution reaction (HER). Selenide platinum ($PtSe_2$) is a typical 1T phase hexagonal lattice structure with P-3m1 space group [7]. Owing to layer-dependent band gap evolution, the band gap of $PtSe_2$ will fall down to zero when the layer number is more than three layers [8, 9], which is an alternative material for infrared photodetection [8], large-area thin-film devices, mid-infrared polarizers and polarization sensors. Several works have reported the chemical vapor deposition growth of $PtSe_2$ crystals on various substrates, such as molecular beam epitaxy [10, 11], chemical vapor transport [12, 13] and chemical vapor deposition [14–16]. Most of the feasible approach is thermally assisted selenation of Pt films to obtain large-area $PtSe_2$ film [17–24].

Rui Hao and Qing-Liang Feng contributed equally to this work.

Supplementary Information The online version contains supplementary material available at https://doi.org/10.1007/s12598-021-01877-z.

R. Hao, K.-S. Li*
College of Chemistry and Chemical Engineering, Polymer Research Institute, Xi'an University of Science and Technology, Xi'an 710054, China
e-mail: likanshe@xust.edu.cn

R. Hao, Q.-L. Feng*, X.-J. Wang, Y.-C. Zhang
Key Laboratory of Special Functional and Smart Polymer Materials of MIIT, School of Chemistry and Chemical Engineering, Northwestern Polytechnical University, Xi'an 710072, China
e-mail: fengql@nwpu.edu.cn

Nanowall, a vertically distributed nano-structure, has shown high-aspect ratio with extensive exposure of edge sites. Owing to the unsaturated bond at edge of monolayer structure, nanowall has shown huge advantage in HER, hydrogen storage devices, supercapacitors hydrodesulfurization catalysis, and biological applications. For now, the carbon nanowalls were prepared by microwave plasma chemical vapor deposition (MPCVD) for its applications in field emission displays and energy storage [25], the MoS_2@rGO nanowall has been synthesized as anode materials [26], and vertical and uniform ReS_2 nanowalls were directly grown on a Si/SiO_2 substrate by chemical vapor deposition (CVD) with prominent PHE efficiency under visible light irradiation [27]. However, the mechanism and controlled selenation of the ultra-chemical stable and high-melt point of Pt atoms to obtain $PtSe_2$ are still unclear.

In this work, we reported the thickness and morphology-controlled growth of continuous large-area $PtSe_2$ nanowall films by thermally assisted selenation of pre-deposited metal Pt films. The uniformity, composition and morphology of $PtSe_2$ nanowall films are characterized by Raman spectroscopy, X-ray photoelectron spectroscopy (XPS), atomic force microscopy (AFM), and high-resolution transmission electron microscopy (HRTEM). The dynamic and thermodynamics of growth process are investigated by tuning growth temperature, heating rate, and flow of carrier gas. The $PtSe_2$ nanowall films are transferred on Au film as the working electrodes, and the HER performances of $PtSe_2$ nanowall films are checked with a three-electrode system. The results show low overpotential of 0.3 V at –10 $mA{\cdot}cm^{-2}$, and small Tafel slope of 52 $mV{\cdot}dec^{-1}$ by the well-ordered $PtSe_2$ nanowall films, suggesting the excellent electrocatalytic properties of $PtSe_2$ film for enhanced HER.

2 Experimental

2.1 Synthesis of $PtSe_2$ film

The $PtSe_2$ films were synthesized in a homemade furnace by a CVD method. Pt films were firstly sputtered on the SiO_2/Si substrate by molecular beam epitaxy (MBE). The substrate was placed in the ceramic boat with Pt layer faced up. Se powders (Alfa Aesar, 99.5%, 100 mg) were as sources placed in the boat. The distance between Se and Pt was about 10 cm. Mixed hydrogen (H_2, 1 $ml{\cdot}min^{-1}$) and argon (Ar, 30 $ml{\cdot}min^{-1}$) were both used as carrier gases. The samples were synthesized in a quartz tube at a temperature ranging from 400 to 800 °C with a growth time of 1 h. Finally, the furnace cooled down to room temperature naturally.

2.2 Crystal structure characterization

Optical images were taken on an Olympus BX51 microscope. AFM characterization was carried out with Bruker Multimode 8 system. The crystal structures images were acquired by transmission electron microscopy (TEM, FEI Tecnai G2 F30). The chemical state and composition studies were performed using X-ray photoelectron spectroscopy (XPS, AXIS Ultra DLD) with a basic chamber pressure of 1×10^{-8} Pa and with an Al anode as the X-ray source. The Raman spectrum was collected using a Bruker RFS 100/S spectrometer (laser wavelength of 532 nm).

2.3 Electrochemical measurements

All measurements were performed in a homemade three-chamber electrochemical cell using a CHI660E electrochemical workstation in 0.5 $mol{\cdot}L^{-1}$ H_2SO_4 solution. The $PtSe_2$ films with different growth temperatures and thicknesses were transferred onto Au films, which served as the working electrodes with a platinum (Pt) counter electrode and an Ag/AgCl (saturated KCl) reference electrode (Hach). The electrochemically active surface area (ECSA) was determined using CV by sweeping the potential between 0.12 and 0.32 V (vs. RHE) at different scan rates is as follows: 10, 15, 20, 25, 30, 35, 40, 45 and 50 $mV{\cdot}s^{-1}$. The potentials in this work were referenced to RHE after iR correction using the following equation: $E_{RHE} = E_{Ag/AgCl} + 0.059\ pH + E^{o}_{Ag/AgCl}$, where $E^{o}_{Ag/AgCl}$ is the potential of the Ag/AgCl electrode at 25 °C.

3 Results and discussion

A homemade one-inch tube furnace is used to provide a confined space for increasing the concentration of gaseous Se atoms to accelerate the selenation reaction in Fig. 1a. By controlling growth temperature and thickness of Pt film, a series of continuous $PtSe_2$ nanowall films are obtained. The photograph of as-grown large-area $PtSe_2$ nanowall films on SiO_2/Si substrate with a size of $> 4\ cm^2$ is shown in Fig. 1b, which is prepared by selenation of Pt film with the thickness of about 1 nm. Figure 1c shows the transferred $PtSe_2$ nanowall film on SiO_2/Si substrate with a continuous large-area film. The AFM image is shown in Fig. 1d with a thickness of 2.9 nm, the zoom in image is also shown in Fig. S1, demonstrating the nanowall structure of as-obtained $PtSe_2$ film. The Raman spectrum is shown in Fig. 1e, and the peaks are located at 178 and 210 cm^{-1}, assigned to the E_g and A_{1g} Raman vibration modes of $PtSe_2$ by mechanical exfoliation. XPS spectra show only one couple peak of Pt and Se with the position at around 73.38 and 76.73 eV, and 54.83 and 55.66 eV,

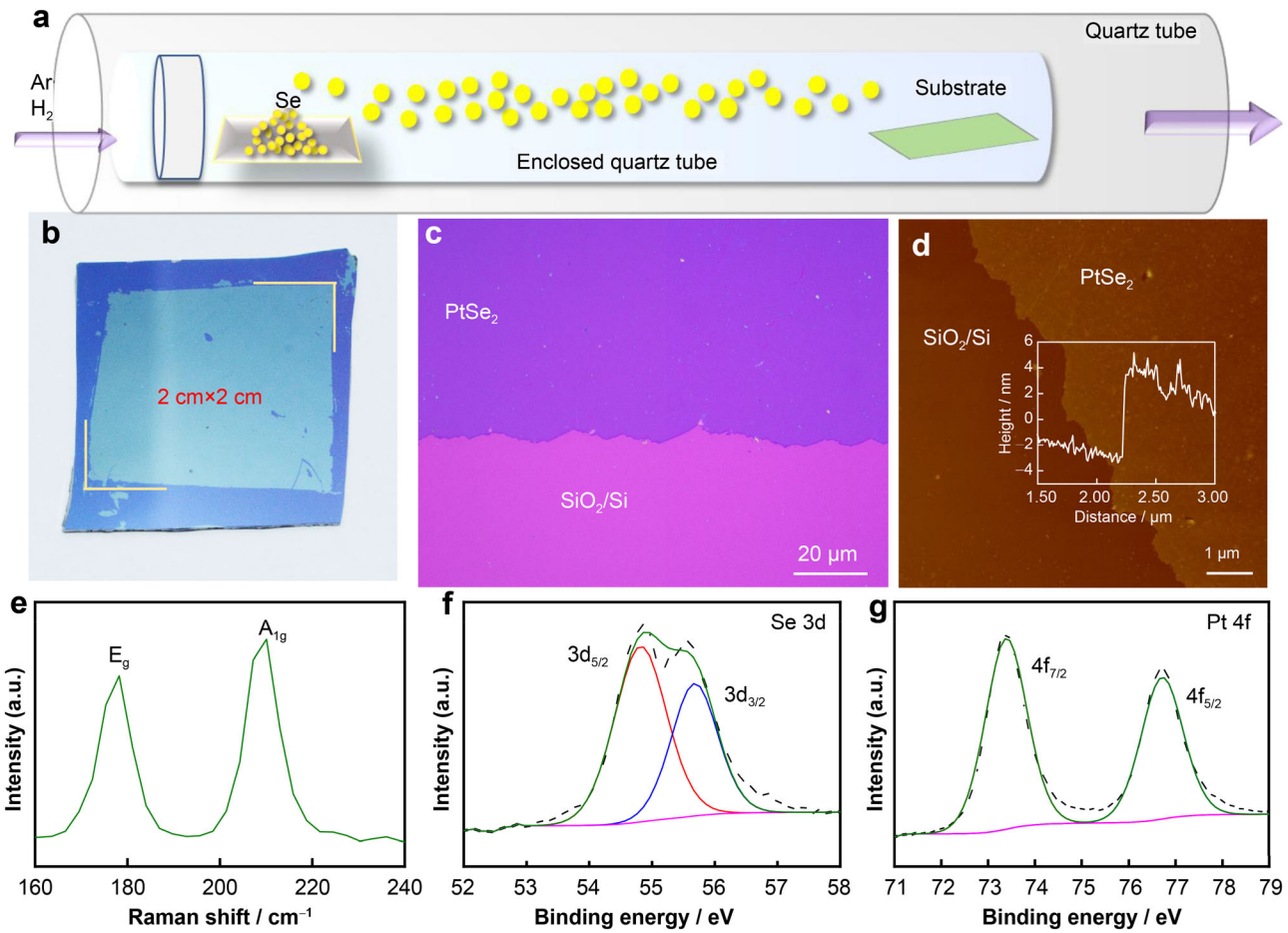

Fig. 1 Controlled growth of $PtSe_2$ films: **a** schematic diagram of modified chemical vapor deposition method to control growth of $PtSe_2$ films; **b** photograph and **c** optical microscopy image of as-obtained $PtSe_2$ films on SiO_2/Si substrates at growth temperature of 650 °C and heating rate of 4 °C·min^{-1}; **d** AFM image of as-grown $PtSe_2$ films; **e** Raman spectrum of as-obtained $PtSe_2$ films; XPS spectra of **f** Se and **g** Pt for as-grown $PtSe_2$ films

which respectively belong to Pt $4f_{7/2}$ and Pt $4f_{5/2}$, and Se $3d_{5/2}$ and Se $3d_{3/2}$, as shown in Fig. 1f, g [24]. The results demonstrated that the valence states of Se and Pt are assigned to –2 and + 4, and the chemical reaction of selenation process is completely finished.

The dynamic and thermodynamics of growth process are investigated by tuning growth temperature, heating rate, and thickness of Pt film. As shown in Fig. 2a, the AFM image is of $PtSe_2$ nanowall films prepared at 400 °C, and a layer of nanoparticles is uniformly distributed on the surface of $PtSe_2$ films. Those particles may be formed due to harder surface migration of $PtSe_2$ clusters at low growth temperature. In Fig. 2b, the continuous film of $PtSe_2$ crystals with high surface roughness is formed at growth temperature of 500 °C but without the nanoparticles. The results demonstrated that the vapor concentration of selenium is excess for selenation reaction, and Pt atoms are fully reacted finally. With the growth temperature up to 600 °C, as shown in Fig. 2c, the Pt clusters are well migrated at the surface; with an increase in the growth temperature, the surface roughness is decreased, and continuous films are formed finally. In Fig. 2d, continuous flat $PtSe_2$ films are obtained with growth temperature of 650 °C, and the morphology has been significantly improved with better crystallinity, higher quality and more uniformity. As the growth temperature is higher than 700 °C, the surface migration process of Pt clusters is further increased, and some Pt atoms will agglomerate into islands and some of as-deposited Pt atoms are also vapor at such high temperature, and the individual $PtSe_2$ nanoflakes are obtained finally in Fig. 2e, f. Figure 2g shows related Raman spectra of as-obtained $PtSe_2$ films with different growth temperatures in Fig. 2a–f. Both the E_g and A_{1g} peaks are redshift with temperature increasing from 400 to 800 °C (Fig. S2).

High-resolution transmission electron microscopy (HRTEM) was used to investigate the morphology evolution of as-obtained $PtSe_2$ crystals. Figure 3a, b shows low-magnification and HRTEM images of $PtSe_2$ film with

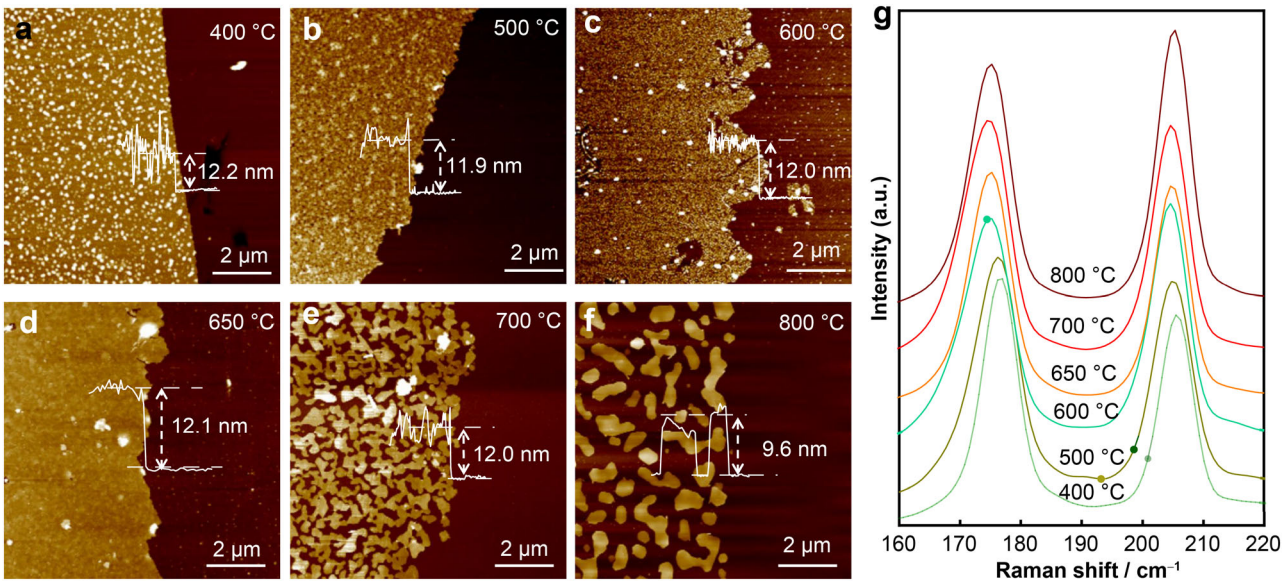

Fig. 2 Thermodynamic investigation of Pt growth: growth of $PtSe_2$ crystals at temperatures of **a** 400 °C, **b** 500 °C, **c** 600 °C, **d** 650 °C, **e** 700 °C, and **f** 800 °C with heating rate of 4 °C·min^{-1}; **g** Raman spectra of as-obtained $PtSe_2$ crystals with different growth temperatures

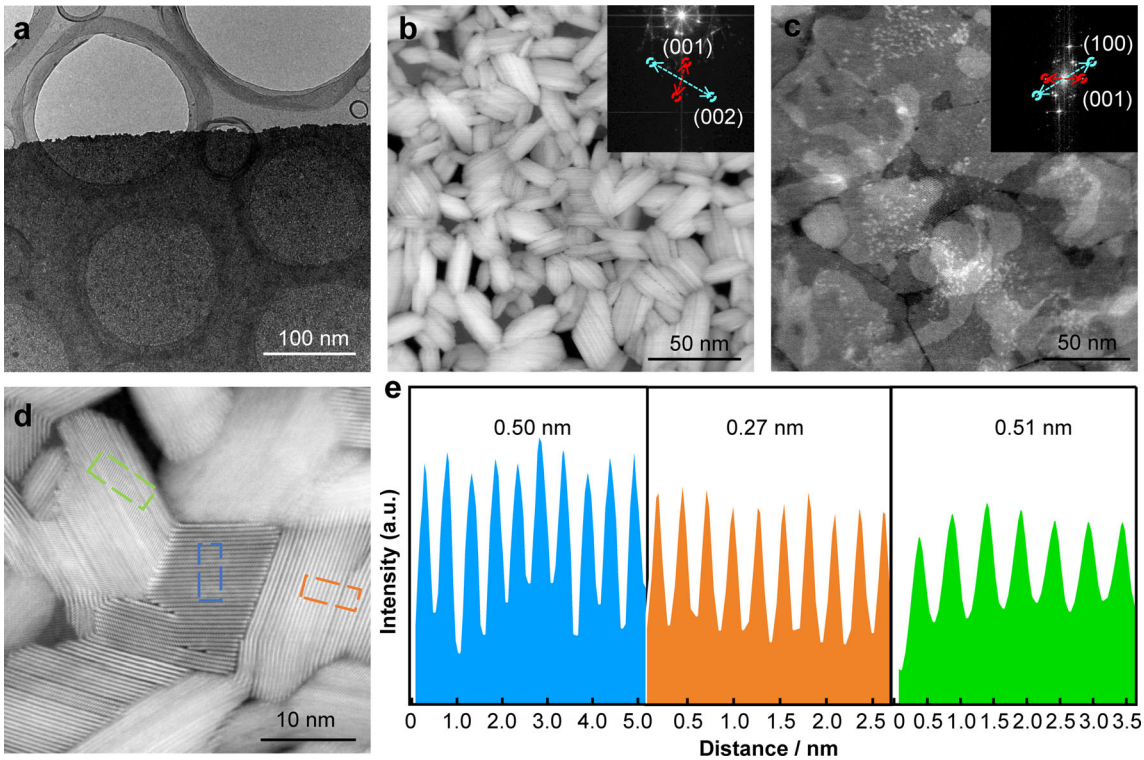

Fig. 3 Structural characterization of as-obtained $PtSe_2$ crystals at different growth temperatures: **a** normal and HRTEM images of as-obtained $PtSe_2$ films with growth temperature of **b** 400 °C and **c** 650 °C and heating rate of 4 °C·min^{-1} (inset images: FFT pattern of as-obtained $PtSe_2$ films); **d** HRTEM image of $PtSe_2$ nanowall films at zoom in area; **e** intensity profiles along three color-dashed lines in **d**

growth temperature of 400 °C and a heating rate of 4 °C·min^{-1}, respectively. The results reveal typical nanowall morphology of as-obtained $PtSe_2$ film with visible lattice fringes. When the growth temperature is up to 650 °C, few-layer $PtSe_2$ continuous films with polycrystalline layered structure are obtained, as shown in Fig. 3c. The domain sizes of each single crystal are almost at 50–70 nm. The insets in Fig. 3b, c are selected area electron diffraction (SAED) patterns of as-obtained $PtSe_2$ nanowall and continuous $PtSe_2$ film, showing the typical crystal diffraction pattern of 1T $PtSe_2$ with (002) of 0.25 nm, (100) of 0.32 nm, and (001) of 0.50 nm. Figure 3d clearly reveals the periodic atom arrangement of nanowall structure for $PtSe_2$ nanowall film at a selected location, which exhibits lattice spacing in different vertical domains as marked by the blue, green, and origin frame. Figure 3e shows the intensity distribution along three color-dashed lines in Fig. 3d, showing that the spacing is 0.50, 0.27 and 0.51 nm, corresponding to (001), (101) and (001) crystal planes of typical 1T $PtSe_2$, respectively.

The temperature-dependent growth behavior of $PtSe_2$ nanowall films was further investigated by analyzing the angle-off nanowalls with different growth temperatures. As shown in Figs. S3–S5, the $PtSe_2$ nanowall films are obtained between 450 and 550 °C. The dynamic of selenation process is also further investigated by tuning heating rate and thickness of Pt film, as shown in Figs. S6–S7. With the heating rate increasing, the real selenate reaction time is decreased at low temperature range, the island agglomeration process is dominative behavior, and the individual $PtSe_2$ nanoflakes are obtained with the heating rate up to 4 °C·min^{-1}.

In Fig. 4a–c, HRTEM images of as-obtained $PtSe_2$ nanowall with temperature of 400, 450 and 550 °C show different angle-off distributions of nanowalls. As shown in Fig. 4d, for the sample grown at low temperature of 400 °C, the values of angle-off are randomly distributed in the range from 30° to 160°, and the values at around 60° and 120° are seemingly more preferred. The angle-off evolution becomes more obvious and preferred to specific values when the growth temperature increases from 450 to 550 °C, which are mostly around at 30°, 60°, 90°, 120° and 150°. As shown in Fig. S6, $PtSe_2$ nanowall films with different thicknesses are grown with different-thickness Pt films. The supposed mechanism for the nanowall-flat evolution is shown in Fig. 4e. The supposed mechanism is that Pt atoms

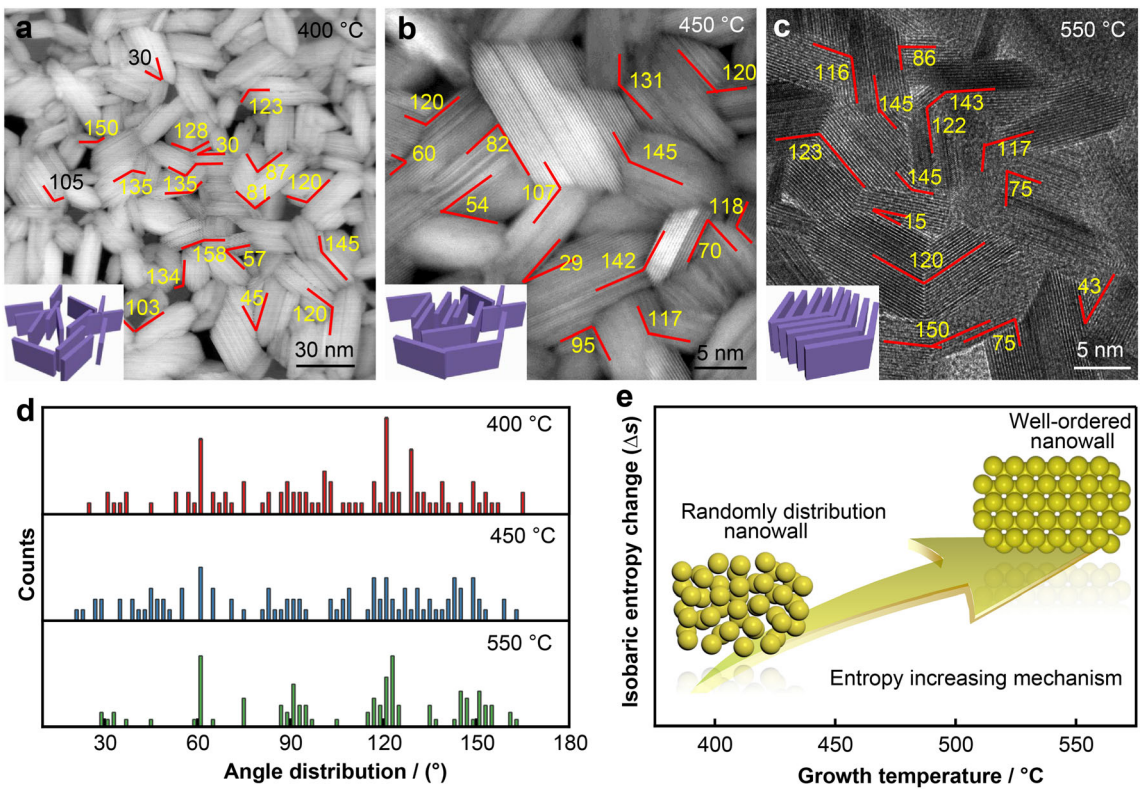

Fig. 4 Investigation of $PtSe_2$ nanowall angle distribution: angle-off analysis of $PtSe_2$ nanowall in HRTEM images with heating rate of 4 °C·min^{-1} and different growth temperatures of **a** 400 °C, **b** 450 °C, and **c** 550 °C; **d** angle-off distribution of nanowall for different growth temperatures; **e** schematic diagram of Pt atoms rearrangement with growth temperature increasing with an entropy increasing process

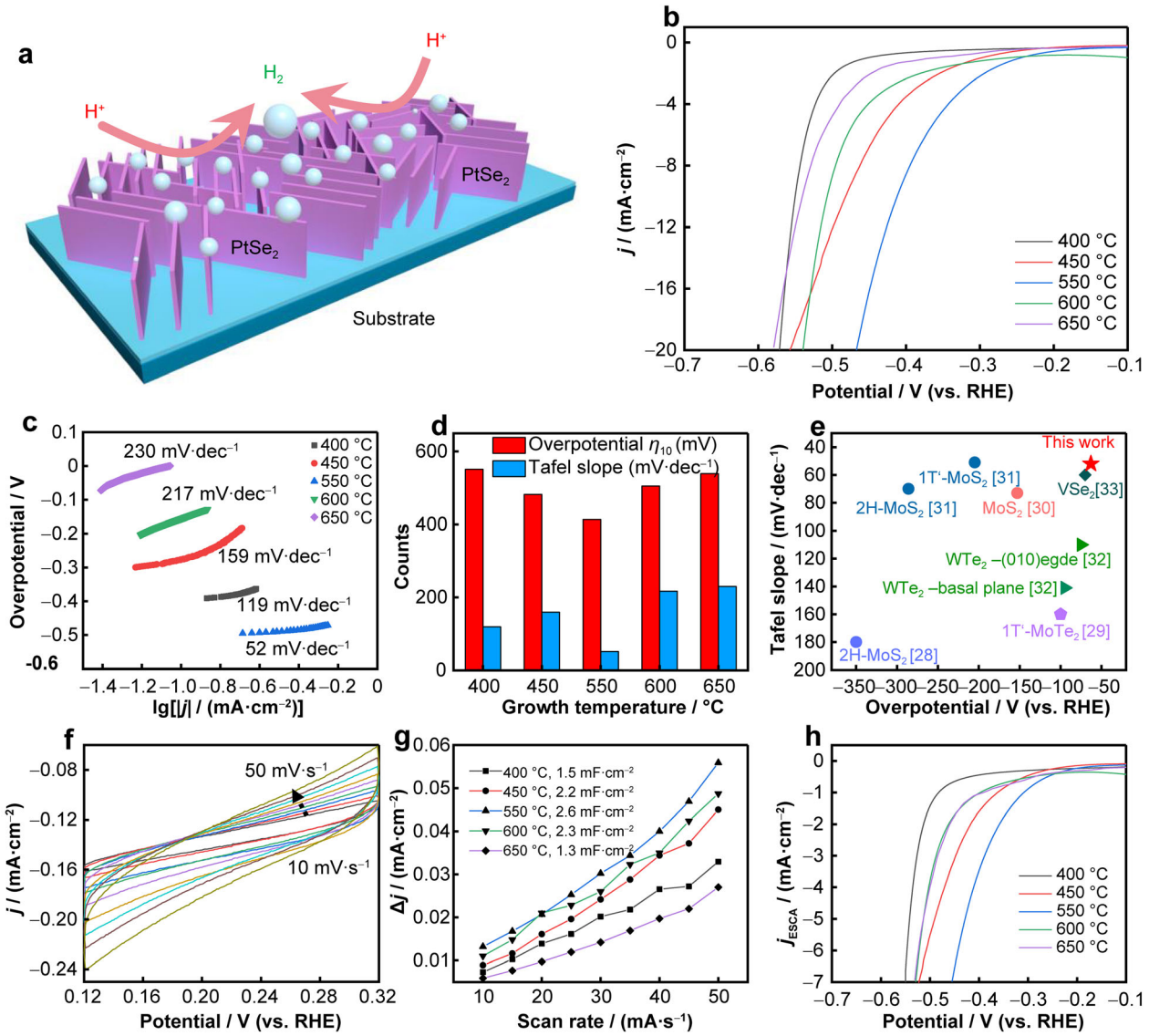

Fig. 5 Electrocatalytic HER activity in 0.5 mol·L^{-1} H_2SO_4: **a** illustration of HER for $PtSe_2$ nanowall films; **b** LSV curves of $PtSe_2$ films with heating rate of 4 °C·min^{-1} and growth temperatures of 400, 450, 550, 600 and 650 °C at a scan rate of 5 mV·s^{-1}; **c** Tafel plots corresponding to samples in **b**; **d** comparison of overpotential at a current density of 10 mA·cm^{-2} and Tafel slope of various samples; **e** comparison of overpotential and Tafel slope in reported work and this work; **f** CV curves of well-ordered $PtSe_2$ nanowall films in region from + 0.12 to + 0.32 V with scan rates from 10 to 50 mV·s^{-1}; **g** plots showing extraction of C_{dl} for estimation of ECSA of various samples; **h** polarization curves normalized by ECSA for various samples with different growth temperatures

on the substrate gradually rearrange to well-ordered structure of Pt (111) surface when the growth temperature increases with such low heating rate, named entropy increasing principle. At the low growth temperature, the surface migration is hard, the selenation reaction of Pt atoms situ occurs, the $PtSe_2$ clusters are in situ piled up under confined space, and $PtSe_2$ nanowalls are formed finally. With the temperature increasing, the surface migration rate of Pt atoms is increased, and the migration barrier is decreased immediately. Owing to the increased surface migration rates of both Pt atoms and as-formed $PtSe_2$ clusters and layered structure which has more space advantage and nanowall structure, it preferred to form flat $PtSe_2$ films. Then, the well-ordered $PtSe_2$ nanowall films are synthesized at high growth temperature of 550 °C and heating rate of 4 °C·min^{-1} finally.

The electrocatalytic HER activity of $PtSe_2$ films with different morphologies is evaluated in 0.5 mol·L^{-1} H_2SO_4 using a standard three-electrode system. Figure 5a illustrates the vertically arranged $PtSe_2$ nanowall structure, which exposes more active sites and unsaturated bonds at the edges and participates in the following catalytic reaction: $2H^+ + 2e^- \rightarrow H_2$, the hydrogen ion obtains electrons to form hydrogen gas. Figure 5b shows polarization

curves of different-morphology $PtSe_2$ films by different growth temperatures (from 400 to 650 °C). The well-ordered $PtSe_2$ nanowall films show the smallest E_{onset} of –181 mV (HER activity in terms of onset potential) and the lowest overpotential of –413 mV at –10 mA·cm^{-2} (η_{10}) (overpotential at 10 mA·cm^{-2}) of the most outstanding HER activity. For a better understanding of HER activity, Tafel plots are used to analyze HER kinetics of as-prepared samples, as shown in Fig. 5c. The Tafel slope of well-ordered $PtSe_2$ nanowall film is 51 mV·dec^{-1}, which is much smaller than those of as-obtained samples with growth temperature of 400, 450, 550, 600 and 650 °C with the Tafel slopes of 119, 159, 51,217 and 230 mV·dec^{-1}, respectively. The smaller Tafel slope indicates the faster HER kinetics with a Volmer–Heyrovsky mechanism [28, 29].

Figure 5d presents HER activities of the samples (η_{10} and Tafel slope), which vividly reveals that well-ordered $PtSe_2$ nanowall films can effectively provide all-round engineering of catalysts for optimized electrocatalytic property [30, 31]. In Fig. 5e, the lowest η_{10} value of ~63 mV and Tafel slope of ~51 mV·dec^{-1} achieved are listed among the excellent values for widely explored 2D few layered TMDSs measured with a microcell setup similar to this work [32–37]. These results demonstrated that the nanowall structure of 2D TMDs uncovers significance of growth temperature for promoting HER kinetics. In addition, ECSA is also estimated by the double-layer capacitance (C_{dl}) of as-obtained samples. Cyclic voltammetry (CV) curves are swept in static solution across non-Faradaic region and C_{dl} is obtained from linear slope of average current density versus scan rate in Fig. 5f–g and Fig. S8. As shown in Fig. 5g, C_{dl} value of well-ordered $PtSe_2$ nanowall films is 2.6 mF·cm^{-2}, maintaining at a high level compared to those of rest samples, which is mainly attributed to abundant active sites at edge of nanowalls [31]. The polarization curves normalized by ECSA for various samples are shown in Fig. 5h, and the results indicate that the well-ordered $PtSe_2$ nanowall films exhibit superior intrinsic HER activity.

We further studied the thickness-dependent HER performance of well-ordered $PtSe_2$ nanowall films. In Fig. 6a, the LSV curves of different samples indicate that the well-ordered $PtSe_2$ nanowalls with thickness of 5.1 nm show the most outstanding HER activity. The corresponding Tafel plots are shown in Fig. 6b, and the $PtSe_2$ nanowall films with thickness of 5.1 nm have the smallest Tafel slope and the fastest HER kinetics. When the thickness increases

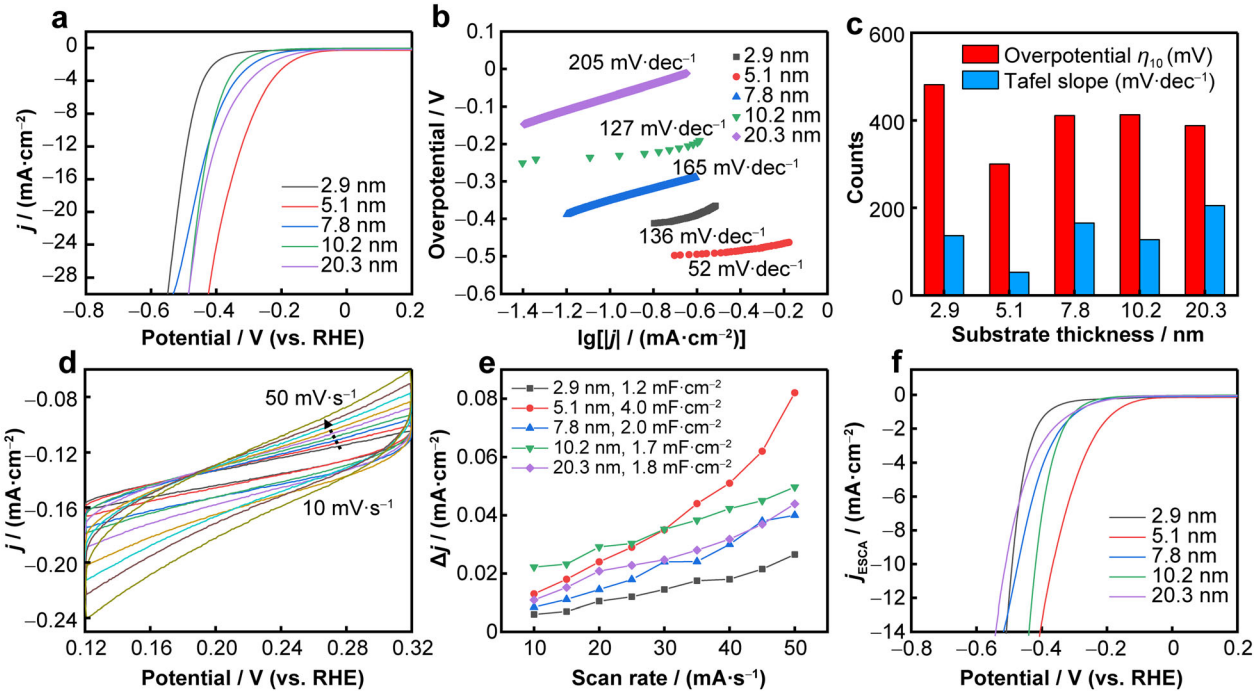

Fig. 6 HER performance of well-ordered $PtSe_2$ nanowall films with different thicknesses: **a** LSV curves of well-ordered $PtSe_2$ films with heating rate of 4 °C·min^{-1} and thickness of 2.9, 5.1, 7.8, 10.2 and 20.3 nm at a scan rate of 5 mV·s^{-1}; **b** Tafel plots corresponding to samples in **a**; **c** comparison of overpotential at a current density of 10 mA·cm^{-2} and Tafel slope of various samples; **d** CV curves of well-ordered $PtSe_2$ nanowall films in region from + 0.12 to + 0.32 V with scan rates from 10 to 50 mV·s^{-1}; **e** plots showing extraction of C_{dl} for estimation of ECSA of various samples; **f** polarization curves normalized by ECSA for various samples with different growth temperatures

from 2.9 to 5.1 nm, more vertically $PtSe_2$ nanowalls are formed, and more edges are exposed, resulting in great enhancement of HER activity. Further increasing the thicknesses from 7.8 to 20.3 nm, multilayer $PtSe_2$ nanowall structures are formed, and the electron transfer pathway in electrode consists of the inside grain boundary of multilayer nanowalls and the interface of electrode. As the results, both the η_{10} value and Tafel slope of HER performance are decreased with the thickness of $PtSe_2$ nanowall increasing, as shown in Fig. 6c. Besides, the intrinsic activities of $PtSe_2$ nanowall films with different substrate thicknesses are also investigated. C_{dl} is obtained from linear slope of average current density versus scan rate, as shown in Fig. 6d and Fig S9. The values of C_{dl} show a trend of first increasing and then decreasing, reaching a maximum of 4.0 $mF{\cdot}cm^{-2}$ at thicknesses of 5.1 nm (Fig. 6e). As shown in Fig. 6f, the normalized LSV curves by ECSA also reveal that the well-ordered $PtSe_2$ nanowall films with thicknesses of 5 nm exhibit the optimal HER activity, which is consistent with the results in Fig. 6a. Besides, we studied a continuous HER process to generate hydrogen through a current–time test at a current density of –10 $mA{\cdot}cm^{-2}$ by applying an overpotential of –0.4 V. The current density shows a plus or minus at range of 7.6% after a long period of 18 h (Fig. S10), indicating prominent stability for HER.

4 Conclusion

In conclusion, we have developed a modified CVD method to obtain high-quality $PtSe_2$ nanowall films and continuous layered $PtSe_2$ films with a large area of 4 cm^2. The continuous $PtSe_2$ nanowall films can be obtained with the growth temperature of below 600 °C, and the continuous layered $PtSe_2$ polycrystalline film when the growth temperature is at around 650 °C. The individual $PtSe_2$ islands will form when the growth temperature is higher than 700 °C. The thickness of $PtSe_2$ nanowall films can be tuned by the thickness of as-deposited Pt films on substrate. The well-ordered $PtSe_2$ nanowall films with growth temperature of 550 °C show the enhanced HER performance, which exposes more edge active sites at the nanowall structure. The highest HER performances are achieved with a η_0 value of $\sim$61 mV and a Tafel slope of $\sim$52 $mV{\cdot}dec^{-1}$ by well-ordered $PtSe_2$ nanowall films with the thickness of 5.1 nm. This work can encourage more works on fabricating 2D TMDs-based nanowall structure for enhanced HER performance.

Acknowledgements This work was financially supported by the National Natural Science Foundation of China (No.51802266), Shaanxi's Key Project of Research and Development Plan (No.2021GY-217), the Research Funds for Interdisciplinary Subject of NWPU (No.19SH0304), and the Fundamental Research Funds for the Central Universities (No.3102017jc01001).

Declarations

Conflict of interests The authors declare that they have no conflict of interest.

References

[1] Lui CH, Li ZQ, Mak KF, Cappelluti E, Heinz TF. Observation of an electrically tunable band gap in trilayer graphene. Nat Phys. 2011;7(12):944.
[2] Fiori G, Bonaccorso F, Iannaccone G, Palacios T, Neumaier D, Seabaugh A, Banerjee SK, Colombo L. Electronics based on two-dimensional materials. Nat Nanotechnol. 2014;9(10):768.
[3] Chen L, Xue F, Li X, Huang X, Wang L, Kou J, Wang ZL. Strain-gated field effect transistor of a MoS_2-ZnO 2D–1D hybrid structure. ACS Nano. 2016;10(1):1546.
[4] Jiang W, Wang X, Chen Y, Wu G, Ba K, Xuan N, Sun Y, Gong P, Bao X, Shen H, Lin T, Meng XJ, Wang J, Sun Z. Large-area high quality $PtSe_2$ thin film with versatile polarity. InfoMat. 2019;1(2):260.
[5] Pi L, Li L, Liu K, Zhang Q, Li H, Zhai T. Recent progress on 2D noble-transition-metal dichalcogenides. Adv Funct Mater. 2019; 29(51):1904932.
[6] Wang FK, Zhai TY. Towards scalable van der Waals heterostructure arrays. Rare Met. 2020;39(4):327.
[7] Yu X, Yu P, Wu D, Singh B, Zeng Q, Lin H, Zhou W, Lin J, Suenaga K, Liu Z, Wang QJ. Atomically thin noble metal dichalcogenide: a broadband mid-infrared semiconductor. Nat Commun. 2018;9:1545.
[8] Zhao Y, Qiao J, Yu Z, Yu P, Xu K, Lau SP, Zhou W, Liu Z, Wang X, Ji W, Chai Y. High-electron-mobility and air-stable 2D layered $PtSe_2$ FETs. Adv Mater. 2017;29(5):1604230.
[9] Kandemir A, Akbali B, Kahraman Z, Badalov SV, Ozcan M, Iyikanat F, Sahin H. Structural, electronic and phononic properties of $PtSe_2$: from monolayer to bulk, Semiconductor Science and Technology. Semicond Sci Technol. 2018; 33 (8): 085002.
[10] Wang Y, Li L, Yao W, Song S, Sun JT, Pan J, Ren X, Li C, Okunishi E, Wang YQ, Wang E, Shao Y, Zhang YY, Yang HT, Schwier EF, Iwasawa H, Shimada K, Taniguchi M, Cheng Z, Zhou S, Du S, Pennycook SJ, Pantelides ST, Gao HJ. Monolayer $PtSe_2$, a new semiconducting transition-metal-dichalcogenide, epitaxially grown by direct selenization of Pt. Nano Lett. 2015; 15(6):4013.
[11] Yan M, Wang E, Zhou X, Zhang G, Zhang H, Zhang K, Yao W, Lu N, Yang S, Wu S, Yoshikawa T, Miyamoto K, Okuda T, Wu Y, Yu P, Duan W, Zhou S. High quality atomically thin $PtSe_2$ films grown by molecular beam epitaxy. 2D Mater. 2017; 4 (4): 045015.
[12] Chia X, Adriano A, Lazar P, Sofer Z, Luxa J, Pumera M. Layered platinum dichalcogenides (PtS_2, $PtSe_2$ and $PtTe_2$) electrocatalysis: monotonic dependence on the chalcogen size. Adv Funct Mater. 2016;26(24):4306.
[13] Hu D, Zhao T, Ping X, Zheng H, Xing L, Liu X, Zheng J, Sun L, Gu L, Tao C, Wang D, Jiao L. Unveiling the layer-dependent catalytic activity of $PtSe_2$ atomic crystals for the hydrogen evolution reaction. Angew Chem Int Ed. 2019;58(21):6977.
[14] Shi J, Huan Y, Hong M, Xu R, Yang P, Zhang Z, Zou X, Zhang Y. Chemical vapor deposition grown large-scale atomically thin platinum diselenide with semimetal-semiconductor transition. ACS Nano. 2019;13(7):8442.

[15] Xu H, Zhang H, Liu Y, Zhang S, Sun Y, Guo Z, Sheng Y, Wang X, Luo C, Wu X, Wang J, Hu W, Xu Z, Sun Q, Zhou P, Shi J, Sun Z, Zhang DW, Bao W. Controlled doping of wafer-scale $PtSe_2$ films for device application. Adv Funct Mater. 2019;29(4): 1805614.
[16] Zhou J, Lin J, Huang X, Zhou Y, Chen Y, Xia J, Wang H, Xie Y, Yu H, Lei J, Wu D, Liu F, Fu Q, Zeng Q, Hsu CH, Yang C, Lu L, Yu T, Shen Z, Lin H, Yakobson BI, Liu Q, Suenaga K, Liu G, Liu Z. A library of atomically thin metal chalcogenides. Nature. 2018;556(7701):335.
[17] O'Brien M, McEvoy N, Motta C, Zheng JY, Berner NC, Kotakoski J, Elibol K, Pennycook TJ, Meyer JC, Yim C, Abid M, Hallam T, Donegan JF, Sanvito S, Duesberg GS. Raman characterization of platinum diselenide thin films. 2D Mater. 2016; 3 (2): 021004.
[18] Shawkat MS, Chung HS, Dev D, Das S, Roy T, Jung Y. Two-dimensional/three-dimensional schottky junction photovoltaic devices realized by the direct CVD growth of vdW 2D $PtSe_2$ layers on silicon. ACS Appl Mater Interfaces. 2019; 11(30):27251.
[19] Yim C, Lee K, McEvoy N, O'Brien M, Riazimehr S, Berner NC, Cullen CP, Kotakoski J, Meyer JC, Lemme MC, Duesberg GS. High-performance hybrid electronic devices from layered $PtSe_2$ films grown at low temperature. ACS Nano. 2016;10(10):9550.
[20] Jakhar A, Kumar P, Moudgil A, Dhyani V, Das S. Optically pumped broadband terahertz modulator based on nanostructured $PtSe_2$ thin films. Adv Opt Mater. 2020;8(7):1901714.
[21] Wang L, Zhang S, McEvoy N, Sun YY, Huang J, Xie Y, Dong N, Zhang X, Kislyakov IM, Nunzi JM, Zhang L, Wang J. Nonlinear optical signatures of the transition from semiconductor to semimetal in $PtSe_2$. Laser Photonics Rev. 2019;13(8): 1900052.
[22] Xie C, Zeng L, Zhang Z, Tsang YH, Luo L, Lee JH. High-performance broadband heterojunction photodetectors based on multilayered $PtSe_2$ directly grown on a Si substrate. Nanoscale. 2018;10(32):15285.
[23] Ansari L, Monaghan S, McEvoy N, Coileáin CÓ, Cullen CP, Lin J, Siris R, Stimpel-Lindner T, Burke KF, Mirabelli G, Duffy R, Caruso E, Nagle RE, Duesberg GS, Hurley PK, Gity F. Quantum confinement-induced semimetal-to-semiconductor evolution in large-area ultra-thin $PtSe_2$ films grown at 400°C. npj 2D Mater. Appl. 2019; 3 (1): 33.
[24] Wagner S, Yim C, McEvoy N, Kataria S, Yokaribas V, Kuc A, Pindl S, Fritzen CP, Heine T, Duesberg GS, Lemme MC. Highly sensitive electromechanical piezoresistive pressure sensors based on large-area layered $PtSe_2$ films. Nano Lett. 2018;18(6): 3738.
[25] Wu Y, Qiao P, Chong T, Shen Z. Carbon nanowalls grown by microwave plasma enhanced chemical vapor deposition. Adv Mater. 2002;14(1):64.
[26] Chen H, Song T, Tang L, Pu X, Li Z, Xu Q, Liu H, Wang Y, Xia Y. In-situ growth of vertically aligned MoS_2 nanowalls on reduced graphene oxide enables a large capacity and highly stable anode for sodium ion storage. J Power Sources. 2020;445: 227271.
[27] Zhang Q, Wang W, Zhang J, Zhu X, Zhang Q, Zhang Y, Ren Z, Song S, Wang J, Ying Z, Wang R, Qiu X, Peng T, Fu L. Highly efficient photocatalytic hydrogen evolution by ReS_2 via a two-electron catalytic reaction. Adv Mater. 2018;30(23): 1707123.
[28] Jiang Y, Yang M, Qu M, Wang Y, Yang Z, Feng Q, Deng X, Shen W, Li M, He R. In situ confinement of Pt within three-dimensional MoO_2@porous carbon for efficient hydrogen evolution. J Mater Chem A. 2020;8(20):10409.
[29] Feng QL, Li M, Wang TX, Chen YP, Wang XJ, Zhang XD, Li XB, Yang ZCY, Feng LP, Zheng JB, Xu H, Zhai TY, Jiang YM. Low-temperature growth of three dimensional ReS_2/ReO_2 metal-semiconductor heterojunctions on graphene/polyimide film for enhanced hydrogen evolution reaction. Appl Catal B Environ. 2020;271:118924.
[30] Ping X, Liang D, Wu Y, Yan X, Zhou S, Hu D, Pan X, Lu P, Jiao L. Activating a two-dimensional $PtSe_2$ basal plane for the hydrogen evolution reaction through the simultaneous generation of atomic vacancies and Pt clusters. Nano Lett. 2021;21(9): 3857.
[31] Lin S, Liu Y, Hu Z, Lu W, Mak CH, Zeng L, Zhao J, Li Y, Yan F, Tsang YH, Zhang X, Lau SP. Tunable active edge sites in $PtSe_2$ films towards hydrogen evolution reaction. Nano Energy. 2017;42:26.
[32] Yu Y, Nam GH, He Q, Wu XJ, Zhang K, Yang Z, Chen J, Ma Q, Zhao M, Liu Z, Ran FR, Wang X, Li H, Huang X, Li B, Xiong Q, Zhang Q, Liu Z, Gu L, Du Y, Huang W, Zhang H. High phase-purity 1T'-MoS_2- and 1T'-$MoSe_2$-layered crystals. Nat Chem. 2018;10(6):638.
[33] You H, Zhuo Z, Lu X, Liu Y, Guo Y, Wang W, Yang H, Wu X, Li H, Zhai T. 1T′-$MoTe_2$-based on-chip electrocatalytic microdevice: a platform to unravel oxidation-dependent electrocatalysis. CCS Chem. 2019;1(5):396.
[34] Jiang Z, Zhou W, Hong A, Guo M, Luo X, Yuan C. MoS_2 moiré superlattice for hydrogen evolution reaction. ACS Energy Lett. 2019;4(12):2830.
[35] Liu L, Wu J, Wu L, Ye M, Liu X, Wang Q, Hou S, Lu P, Sun L, Zheng J, Xing L, Gu L, Jiang X, Xie L, Jiao L. Phase-selective synthesis of 1T' MoS_2 monolayers and heterophase bilayers. Nat Mater. 2018;17(12):1108.
[36] Zhou Y, Silva JL, Woods JM, Pondick JV, Feng Q, Liang Z, Liu W, Lin L, Deng B, Brena B, Xia F, Peng H, Liu Z, Wang H, Araujo CM, Cha JJ. Revealing the contribution of individual factors to hydrogen evolution reaction catalytic activity. Adv Mater. 2018;30(18):1706076.
[37] Yan M, Pan X, Wang P, Chen F, He L, Jiang G, Wang J, Liu JZ, Xu X, Liao X, Yang J, Mai L. Field-effect tuned adsorption dynamics of VSe_2 nanosheets for enhanced hydrogen evolution reaction. Nano Lett. 2017;17(7):4109.